Enhancing the HVRT capability of DFIG-based wind farms using cooperative rotor-side SMES considering blocking fault of LCC-HVDC system

Xie, Qi; Zheng, Zixuan ; Xiao, Xianyong; Huang, Chunjun; Zheng, Jiaqu ; Ren, Jie

Published in:
CSEE Journal of Power and Energy Systems

Link to article, DOI:
10.17775/CSEEJPES.2020.01690

Publication date:
2021

Document Version
Peer reviewed version

Enhancing the HVRT Capability of DFIG-based Wind Farms Using Cooperative Rotor-Side SMES Considering Blocking Fault of LCC-HVDC System

Qi Xie, Zixuan Zheng, *Member, IEEE*, Xianyong Xiao, *Senior Member, IEEE,* Chunjun Huang, Jiaqu Zheng, and Jie Ren

***Abstract*—Line-commutated converter based high voltage direct current (LCC-HVDC) has been applied for transferring bulk power from wind farms to load center through long distance in many countries. When the blocking fault of LCC-HVDC system occurs, the surplus reactive power accumulated at the sending end will lead to an overvoltage thus causing the disconnection of wind turbines. To maintain the reliable connection of wind turbines and ensure the stability of power system, this paper introduce one superconducting magnetic energy storage (SMES) unit to connect in parallel with the rotor side of doubly fed induction generator (DFIG). By controlling the energy side converter and rotor side converter to inject demagnetizing current and reactive current into the rotor, the proposed scheme can effectively stabilize key parameters of wind turbine and provide desirable reactive power support, showing a favorable high voltage ride through (HVRT) performance. Several cases based on PSCAD/EMTDC & MATLAB/Simulink co-simulation together with economic analysis are conducted to demonstrate the feasibility and superiority of the proposed scheme on enhancing HVRT capability of DFIG-based wind farms.**

***Index Terms*—HVDC blocking fault, DFIG, superconducting magnetic energy storage, HVRT.**

I. Introduction

TOTAL capacity for wind energy globally in 2019 is over 651 GW, with an increase of 10 percent compared to 2018 [1]. However, most wind farms are located at remote areas and far away from load center. Line-commutated converter based high voltage direct current (LCC-HVDC) transmission system is considered as one of the best ways to economically transmit the bulk wind power through such long distance [2]-[4]. To ensure the normal operation of LCC-HVDC transmission system, the VAR compensators are needed as the converter station will consume a large of reactive power. When the LCC-HVDC blocking fault occurs, the long switch process causes the surplus reactive power capacity of the installed VAR compensators cannot be consumed timely, causing the overvoltage at sending AC system [5]. The overvoltage may cause the cascading trip-off of DFIG -based wind farm, leading to power system voltage instability [6]-[7]. In order to ensure voltage stability and evade critical incidents, DFIG-based wind farms are required to maintain reliable grid-connection under such overvoltage.

Numerous researches have been conducted aiming at meeting the high voltage ride through (HVRT) requirements for wind turbine and improving the stability of power system under LCC-HVDC blocking fault. Existing solutions for enhancing HVRT capability of DFIG connected to LCC-HVDC system can be divided into three categories: system side scheme, DFIG side scheme, and coordinated control scheme.

System side scheme try to mitigate the overvoltage at power system level. In [8], coordinated control strategy of generator shedding by stability control system and filters switched-off by pole control system is proposed to decrease the transient overvoltage caused by DC blocking. In [9], strategies such as improving short circuit capacity, strengthening grid structure, and improving voltage adaptability of wind farms are proposed to preventing cascading tripping of wind farms. However, this scheme cannot completely prevent wind farm from tripping off caused by transient overvoltage.

DFIG side scheme is to enhance the HVRT capability of DFIG itself by improving converter control. Resonance controller, virtual impedance control, enhanced hysteresis-based current regulator are proposed to improve the HVRT capability of wind farms in [10]-[12]. Demagnetization control is a well-known technique, which can reduce the rotor voltage by injecting demagnetizing current that opposite to the magnetic flux [13]. In [14], a *P*-*Q* coordination based HVRT strategy is proposed to suppress transient overvoltage, in which the *Q*-*V* control is coordinated with the *P*-*V* de-loading control to achieve the maximum reactive power capacity. However, DFIG will still face an overvoltage, together with decreased

This work was supported by the National Natural Science Foundation of China (No.51907134).

Q. Xie, Z. X. Zheng (corresponding author, e-mail: scuzzx@163.com), X. Y. Xiao, J. Q. Zheng, and J. Ren are with the College of Electrical Engineering, Sichuan University, Chengdu 610065, China.

C. J. Huang is with the Center for Electric Power and Energy, Technical University of Denmark, 4000 Roskilde, Denmark.

DOI: 10.17775/CSEEJPES.2020.01690

DFIG active power and high rotor voltage. Although the improved control scheme has a relatively low cost, the control ability is limited thus cannot ride through severe fault.

Coordinated control scheme is to fulfill HVRT by coordinating DFIG and additional equipment. Many auxiliary hardware devices have been utilized for enhancing the HVRT capability of DFIG, including the series dynamic resistor, dynamic voltage restorer (DVR), STATCOM, unified power flow controller (UPFC), and SVC [15-19]. Zhang proposed a HVRT strategy in [20]. By coordinating the VAR compensators, DFIG-based wind farm, HVDC system converter, and synchronous compensator, the proposed scheme can restrain the overvoltage significantly. Similarly, Han proposed a collaborative control strategy by putting into static var compensators and cutting off the sending AC filters on the basis of different response times [21]. The HVRT control strategy based on the coordination of wind turbine with division of controllable domain and STATCOM is proposed in [22]. These schemes perform well when dealing with wind farm overvoltage problems caused by HVDC blocking, but they need the help of fast VAR compensators. Moreover, the fault ride through capability of DFIG itself has not been significantly improved.

Superconducting magnetic energy storage system (SMES) has the advantages of fast response speed, long service life, large power density, etc. Some researchers pointed out that the total investment cost of the compensation device based on SMES is relatively acceptable [23]-[24], and its applications in the fault ride-through problem of DFIG have been already proved to have practical value [25]-[27]. Considering the advantages of SMES and the drawbacks of existing HVRT schemes, this paper propose a cooperative strategy of SMES device and demagnetization control to enhance the HVRT capability of DFIG-based wind farms. One SMES unit integrated with the energy side converter (ESC) is introduced to connect in parallel with the rotor side of DFIG. By coordinating energy side converter with rotor side converter (RSC) to inject demagnetizing current and reactive current into rotor，the key parameters of wind turbine can be effectively stabilized and providing desirable reactive power support. Compared with the existing scheme, the proposed scheme has faster response speed due to the characteristics of SMES, stronger fault ride-through and reactive power support capability.

II. Mechanism Of Overvoltage Caused By HVDC Blocking Faults

The typical LCC-HVDC sending system configuration is shown in Fig. 1 [20]. An equivalent DFIG and a synchronous generator is used to represent the wind farm and sending AC system, respectively. The VAR compensators here are AC filters and fixed capacitor. To simplify the overvoltage analysis, the equivalent circuit shown in Fig. 2 is used.

There is no reactive power exchange between the AC system and the LCC-HVDC system normally as the reactive power that rectifier consumed is balanced by the VAR compensators. When the blocking fault occurs, the transmitted active power and the consumed reactive power become zero, but the VAR compensators are still generating reactive power due to their long switch process. The mismatched reactive power will lead to an overvoltage at the point of common coupling (PCC). The overvoltage makes the VAR compensators generate more reactive power. Consequently, the voltage will be even higher.

Typically, the switching process of the mechanical fixed capacitor mostly sustains 200 ms. For STATCOM, since the dual closed-loop control scheme is usually used, its dynamic reactive power response is relatively slow, which is about 100 ms. Therefore, the overvoltage under the LCC-HVDC blocking faults is inevitable and the wind generator would withstand a high voltage for at least 100–200 ms. When the fault is not cleared in time, the overvoltage may last longer.

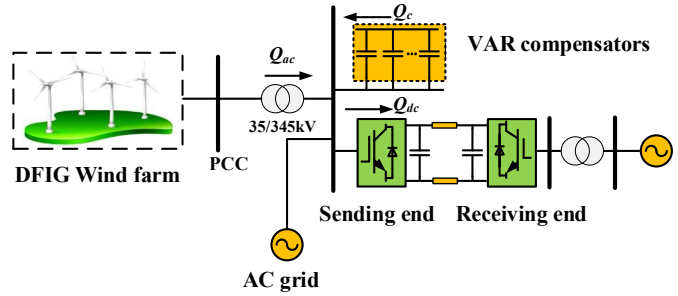

Fig. 1 Structure of LCC-HVDC system

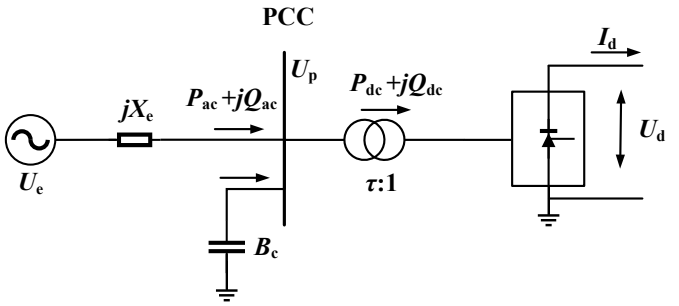

Fig. 2 Simplified equivalent circuit of the LCC-HVDC system

(1) is used to calculate the transient overvoltage [28].

$$U_p' = \frac{U_e - U_e\sqrt{1-\dfrac{4kQ_{cN}}{P_{dN}SCR}}}{\dfrac{2Q_{cN}}{P_{dN}SCR}} \tag{1}$$

where k is a coefficient which is 1 for bipolar blocking and 0.5 for mono-polar blocking. SCR is the short circuit ratio and Q_{cN} is blocking capacity. According to (1), the maximum overvoltage caused by the mono-polar blocking and the bipolar blocking are 1.213 p.u. and 1.44 p.u. respectively [28].

Therefore, it is very necessary to enhance the high voltage ride through capability of DFIG, meet the grid code of wind farms and avoid the overvoltage affecting the safety and stability of the power system.

III. DFIG Model Connected With SMES And Cooperative Transient Control Strategy

A. DFIG model connected with rotor side SMES

As shown in Fig. 3, the stator of DFIG is directly connected to the grid via a step-up transformer, the rotor is connected to a back-to-back PWM converter, and the SMES is connected to the rotor of DFIG in parallel with the rotor-side converter. At steady state, the ESC capacitor is connected in parallel with the

DFIG DC bus, and the switch *S* is closed. In this case, the ESC reference signal is 0, and the ESC do not exchange power with rotor, reducing harmonic injection into the rotor winding. When the LCC-HVDC blocking fault occurs, the switch *S* which connected with the DC bus is quickly opened, and the SMES is connected in parallel with the RSC in this situation. The energy stored in the SMES generates demagnetizing current and reactive current through the ESC and cooperates with the demagnetizing and reactive current generated by the RSC injected into the rotor winding.

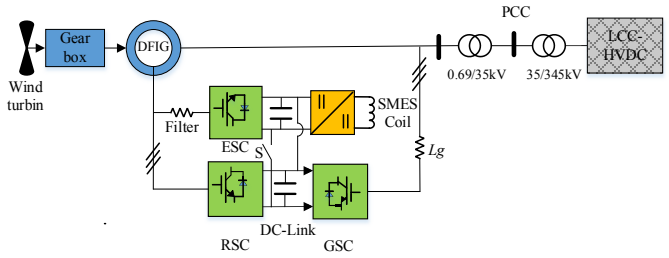

Fig. 3 DFIG wind energy conversion system with rotor side SMES

B. Demagnetization control strategy

When the voltage swell occurs, the dc component of the stator flux linkage is generated, and it is accompanied by a negative sequence component in the case of asymmetric faults. Under the coupling effect between stator and rotor, these components of the stator flux linkage will induce a large electromotive force on the rotor side, that is, the rotor overvoltage. Because the rotor leakage resistance and resistance are relatively small, this overvoltage will produce an overcurrent. The overvoltage and overcurrent cause the RSC to lose the decoupling control of DFIG, which further aggravates the power imbalance of the converter, resulting in overvoltage and electromagnetic torque oscillation of the dc bus, and finally causing DFIG to trip-off. Therefore, the key to realize DFIG HVRT is to accelerate the decrease of the dc and negative sequence component of the stator flux, reduce the overvoltage and overcurrent of the rotor, and avoid the RSC losing control.

The positive sequence, negative sequence and dc components of the stator flux are generated in the case of voltage swell. The decrease of the dc and negative sequence components of the stator flux is accelerated by generating flux components in the RSC and SMES that are opposite to the dc and negative sequence components of the stator flux.

The stator flux is defined as:

$$\psi_{sdq} = L_s i_{sdq} + L_m i_{rdq} = L_m i_{msdq} \tag{2}$$

where i_{msdq} is stator equivalent excitation current, $i_{msdq}=i_{sdq}L_s/L_m+i_{rdq}$, and:

$$\begin{cases} i_{sdq} = \dfrac{L_m}{L_s}\left(i_{msdq} - i_{rdq}\right) \\ \psi_{rdq} = \dfrac{L_m^2}{L_s} i_{msdq} + \sigma L_r i_{rdq} \end{cases} \tag{3}$$

Then, the traditional vector control voltage equation under dq frame can be obtained as follows:

$$\begin{cases} u_{rd} = R_r i_{rd} + \sigma L_r \dfrac{di_{rd}}{dt} - \omega_m \psi_{rq} \\ u_{rq} = R_r i_{rq} + \sigma L_r \dfrac{di_{rq}}{dt} + \omega_m \psi_{rd} \end{cases} \tag{4}$$

The rotor flux is defined as follows:

$$\psi_r = \frac{L_m}{L_s}\psi_s + \sigma L_r i_r \approx \frac{L_m}{L_s}\left(\psi_{s1} + \psi_{s2} + \psi_{s3}\right) + \sigma L_r i_r \tag{5}$$

According to (5), the rotor induced electromotive force can be reduced by injecting flux components that contrary to the dc and negative sequence component of the stator flux by controlling the rotor current.

$$i_{r\text{demaref}} = i_{r2\text{ref}} + i_{rn\text{ref}} = -\frac{\psi_{s2}}{\sigma L_r} - \frac{\psi_{sn}}{\sigma L_r} \tag{6}$$

where, $i_{r\text{demaref}}$ is the reference value of total demagnetization current; $i_{r2\text{ref}}$ is the reference value of negative sequence demagnetization current. $i_{rn\text{ref}}$ is the reference value of dc demagnetization current.

The SMES and RSC together provide the demagnetization current when the voltage swell occurs, i.e.

$$i_{r\text{demaref}} = i'_{r\text{RSC}} + i'_{r\text{ESC}} \tag{7}$$

where, $i'_{r\text{RSC}}$ is the demagnetization current provided by the RSC, $i'_{r\text{ESC}}$ is the demagnetization current provided by the ESC, and the rotor closed-loop current control after adding the demagnetization current is:

$$\begin{cases} i''_{rd} = i_{rddemaref} + i_{rd} \\ i''_{rq} = i_{rqdemaref} + i_{rq} \end{cases} \tag{8}$$

C. DFIG rotor-side converter control strategy

According to the German E.ON standard for HVRT, DFIG should also provide reactive power on the premise that it ride through the fault. Specifically, when the voltage rises to 1.1 or above, the DFIG is required to provide at least 2% reactive power once voltage increases by per 1% to compensate the grid voltage. The reactive current is provided equally by the RSC and SMES.

$$\begin{cases} i_{rQ} = -2\times(v_s - 1.1)I_N \\ i_{rQ} = i_{rQRSC} + i_{rQESC} \end{cases} \tag{9}$$

where i_{rQ} is the total reactive current injected into the rotor; i_{rQRSC} is the reactive current provided by the RSC. i_{rQESC} is the reactive current provided by the ESC.

Considering both demagnetization current and reactive current, the rotor reference current is:

$$\begin{cases} i'_{rd} = i''_{rd} \\ i'_{rq} = i''_{rq} + i_{rQ} \end{cases} \tag{10}$$

Represent the rotor flux by stator voltage and rotor current:

$$\begin{cases} \psi_{rd} = \sigma L_r i_{rd} \\ \psi_{rq} = -\dfrac{L_m}{\omega_s L_s} u_s + \sigma L_r i_{rq} \end{cases} \tag{11}$$

Substitute (10) and (11) into (4) to obtain the RSC closed-loop control equation. The control diagram is shown in Fig. 4.

$$\begin{cases} u_{rd}^{*} = R_r i'_{rd} + \sigma L_r \dfrac{\mathrm{d}i'_{rd}}{dt} - \omega_m (-\dfrac{L_m}{\omega_s L_s} u_s + \sigma L_r i_{rq}) \\ u_{rq}^{*} = R_r i'_{rq} + \sigma L_r \dfrac{\mathrm{d}i'_{rq}}{dt} + \omega_m \sigma L_r i_{rd} \end{cases} \tag{12}$$

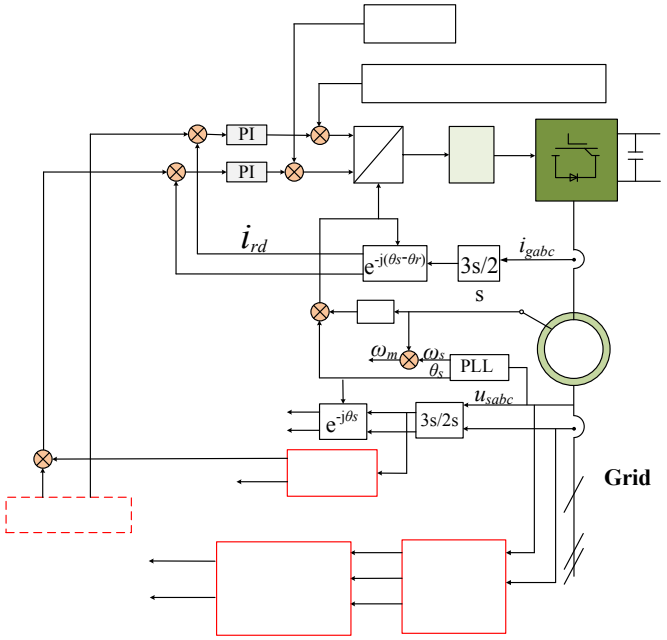

Fig. 4 Control diagram of rotor-side converter

According to Fig. 4, when the voltage swell occurs, the fault identification algorithm proposed in [29] is adopted to quickly and accurately calculate the positive and negative sequence component amplitude of the grid voltage, so as to generate the reference signal of injected reactive current. Flux sequence component separation algorithm is adopted to calculate the demagnetization reference current. The dq-axes rotor voltage references are got by two independent PI controller. Then generate the RSC switch signal by PWM modulator.

D. SMES power flow and its control strategy

The equivalent circuit diagram is shown in Fig. 5. The switch is equivalent to ideal switch S_1, S_3, and a series resistance R_{on}; The diode is equivalent to ideal diode D_2, D_4, a series equivalent resistance R_d, and a series equivalent voltage source U_d. During charging stage, the current path is R_{on}, S_1, L_{SC}, R_{on}, and S_3. During energy storage stage, the current path is R_{on}, S_1, L_{sc}, R_d, and D_4. During discharge stage, the current path is R_d, D_2, L_{SC}, D_4, and R_d, then injects demagnetization current and reactive current into the rotor through ESC.

Ignoring the loss of superconductor and refrigeration device, the current and voltage equation at steady state are:

$$\begin{cases} i(t) = i_C(t) \\ u_{dc} = \dfrac{1}{C}\int_0^t i_C(t)\mathrm{d}t \end{cases} \tag{13}$$

$$L_{sc}\frac{\mathrm{d}i_L(t)}{\mathrm{d}t} + i_L(t)R_{on} + i_L(t)R_d + U_d = 0 \tag{14}$$

where i(t) is the equivalent DC output current, i_C(t) is the working current of the DC capacitor, u_{dc} is the initial voltage of the DC capacitor. i_L(t) is the working current of the superconductor.

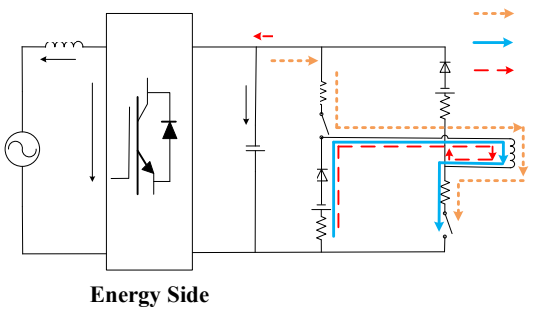

Fig. 5 The equivalent circuit diagram of SMES

When voltage swell occurs, SMES provides demagnetization current and reactive current to DFIG rotor. SMES is connected in parallel with the RSC in this case. Ignoring the loss of SMES and RSC resistance, the parallel equivalent inductance is:

$$L'_r = \frac{L_r L_{sc}}{L_r + L_{sc}} \tag{15}$$

Ignoring rotor resistance R_r:

$$\frac{L_m}{L_s}\frac{\mathrm{d}\psi_{sdq}}{\mathrm{d}t} + \sigma L_r \frac{\mathrm{d}i'_{rdq}}{\mathrm{d}t} = L'_r \frac{\mathrm{d}i'_{rdq}}{\mathrm{d}t} \tag{16}$$

Thus, the rotor current can be expressed as:

$$\left|i'_{rdq}\right| = \frac{L_s}{L_m}\left(\frac{L_r L_{sc}}{L_r + L_{sc}} - \sigma L_r\right)\left|\psi_{sdq}\right| \tag{17}$$

The rotor side voltage and current can withstand a maximum of 2.0 p.u., demagnetization/reactive power current and rotor side voltage are limited by this value:

$$\begin{cases} \left|i_r\right| \le I_{r\max} \\ \left|u_r\right| = \dfrac{L_r L_{sc}}{\sigma L_r L_r + L_{sc} + L_r L_{sc}}\left|e_r\right| \le U_{r\max} \end{cases} \tag{18}$$

Energy is transferred to the converter through chopper circuit, the reactive power exchanged between ESC and rotor is Q_{ESC}:

$$Q_{ESC} = u_r \frac{u_r - u_{rESC}}{jX_{LESC}} = \frac{u_r u_{rESC}\cos\delta}{X_{LESC}} - \frac{u_r^2}{X_{LESC}} \tag{19}$$

where, u_{rESC} is the AC side voltage of the converter; X_{LESC} is AC side inductance of the converter; δ is the phase difference between u_{rESC} and u_r; When the ESC adopts PWM control, the voltage relationship between AC side and DC side is:

$$u_{rESC} = M\sqrt{\frac{3}{2}}\frac{u_{dc}}{2}\angle\delta \tag{20}$$

where M is modulation ratio. When adopting space vector PWM, its maximum value M_{max}=1.15. Thus, (19) can be expressed as:

$$Q_{ESC} = M\sqrt{\frac{3}{2}}\frac{u_{dc}}{2}\frac{u_r\cos\delta}{X_{LESC}} - \frac{u_r^2}{X_{LESC}} \tag{21}$$

Equation (21) indicate that the reactive power provided by SMES can be controlled by controlling the output voltage u_{rESC} of the ESC. The inner current control of SMES is shown in Fig. 6. When voltage swell occurs, failure detection algorithm is applied to calculate the required reactive current. The flux sequence component separation algorithm is adopted to calculate the demagnetization current reference signal. The reactive current reference signal and the demagnetization

current signal are used to obtain voltage signals through two independent closed-loop controller. The ESC switch signal is generated by PMW, then ESC and RSC cooperated to complete DFIG HVRT.

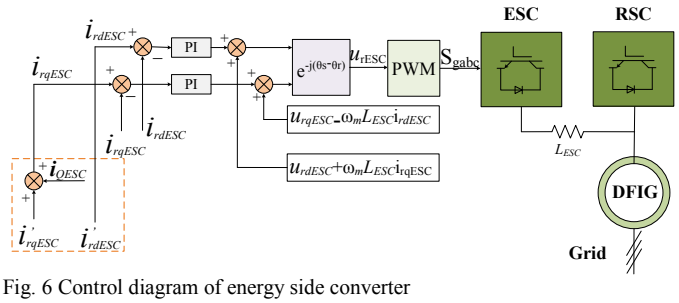

Fig. 6 Control diagram of energy side converter

IV. Simulation Analysis

A. System parameters

In order to verify that the proposed scheme can enhance the HVRT capability of DFIG under LCC-HVDC blocking fault, a LCC-HVDC transmission system connected DFIG wind farm are built in PSCAD/EMTDC, and a 1.5 MW DFIG with rotor-side SMES is built in MATLAB / Simulink, respectively, as illustrated in Fig. 1 and Fig. 3. The VAR compensators here are 13th filter, 11th filter, and shunt capacitors. Their capacities are 252 Mvar, 252 Mvar, and 125 Mvar, respectively. Detailed parameters are shown in Table I and Table II [30]. The design of SMES can be seen in our previous work in [31], [32].

The bipolar blocking faults occurs at t=0.3 s and is simulated in PSCAD/EMTDC. Transient voltage at 345 kV coupling point under the fault is shown in Fig. 7, it can be seen the voltage quickly rise to over 1.3 p.u.. Then, this transient voltage is simulated in MATLAB/Simulink to study the DFIG response.

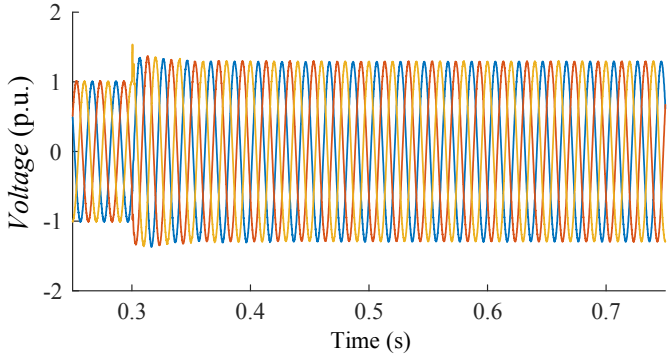

Fig. 7 Transient voltage at 345 kV coupling point

TABLE I
LCC-HVDC System Parameters

Parameter	Value	Parameter	Value
Rated voltage/kV	500	Wind speed/(m/s)	11
Rated DC current/kA	1	DFIG active power/MW	200
Reactive power compensation/MVar	629	DFIG power/MVA	250
SCR of sending system	2.5	Base frequency	50 Hz
SCR of receiving system	3		

TABLE II
DFIG and SMES Parameters

	Parameter	Value
DFIG	Capacity/MW	1.5
	Stator/Rotor voltage/V	690/1725
	Frequency/Hz	50
	DC bus voltage/V	1200
	pole pairs	2
	Stator/Rotor resistance/pu	0.007/0.005
	Stator/Rotor inductance /pu	3.071/3.056
SMES	SC inductance/H	0.3
	SC initial current/A	1500
	SMES DC link capacitor/μF	100

B. Comparison of DFIG response

In this section, a comparison study is conducted among the following three cases: 1) without protection; 2): demagnetization control, and 3) proposed cooperative scheme. The simulation results are illustrated in Fig. 8.

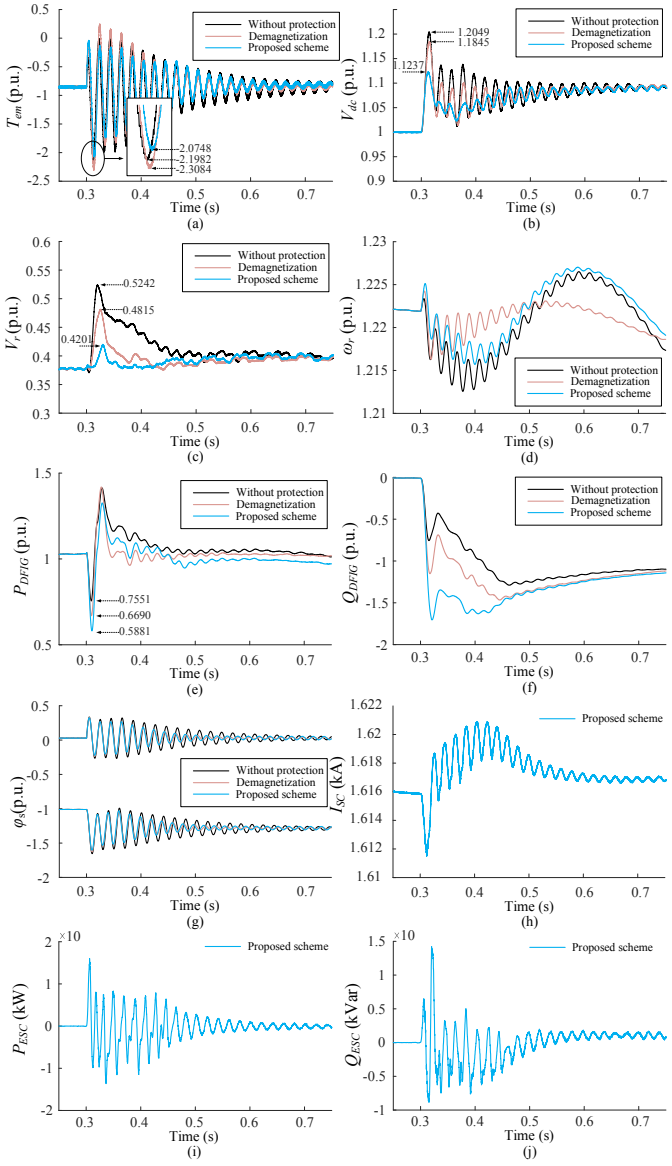

Fig. 8 Simulation results. (a) Electromagnetic torque. (b) Voltage of DC link. (c) RSC voltage. (d) Rotor speed. (e) Active power of DFIG. (f) Reactive power of DFIG. (g) Stator flux dq components. (h) Superconducting coil current. (i) Active power of ESC. (j) Reactive power of ESC

It can be observed from Fig. 8 that when the blocking fault occurs: 1) both electromagnetic torque and voltage of DC link experience an oscillation and have a peak value, proposed scheme has the best performance in mitigating the oscillation and the peak values; 2) the rotor voltage increases to 0.5242 p.u.

without protection during the fault, and proposed scheme can reduce the voltage to 0.4201 p.u., while demagnetization can only limit the voltage to 0.4815 p.u.; 3) rotor speed changes very little in all three cases, the proposed scheme has a certain effect in suppressing the rotor speed oscillation while demagnetization control performs best. 4) Stator flux dq components continuous oscillate during the fault, causing electromagnetic torque oscillation and DC bus overvoltage. Both case 2 and case 3 can mitigate the stator flux oscillation; 5) DFIG active power drop to 0.5881 p.u. under proposed scheme. For case 1 and 2, the value is 0.7551 and 0.669, respectively. Therefore, the proposed scheme can absorb more reactive power to reduce the PCC voltage than the other two schemes. 6) Stator flux oscillation is weakened under both case 2 and 3.

The SMES behaviors during the fault is shown in Fig. 8 (h) to (j). Since the stator flux is oscillated during the fault, superconducting coil current, active power, and reactive power provided by SMES are oscillated continuously, but their consistent trend is to provide demagnetization current and reactive current to help DFIG ride through the fault. Voltage at PCC is shown in Fig. 9. It shows that the proposed scheme can decrease the transient overvoltage at PCC, and more DFIGs, better performance. The peak value under these scenes are shown in Table III. Compared with Spain HVRT codes, when the fault sustain less than 250 ms, 2×1.5 MW DFIGs equipped with SMES can meet the grid code. For the fault longer than 250 ms, more than 7 DFIGs equipped with SMES are needed to meet the requirements. In summary, proposed scheme has the best performance in stabilize key parameters of wind turbine and can effectively suppress transient overvoltage to help DFIG ride through the high voltage process under HVDC blocking fault.

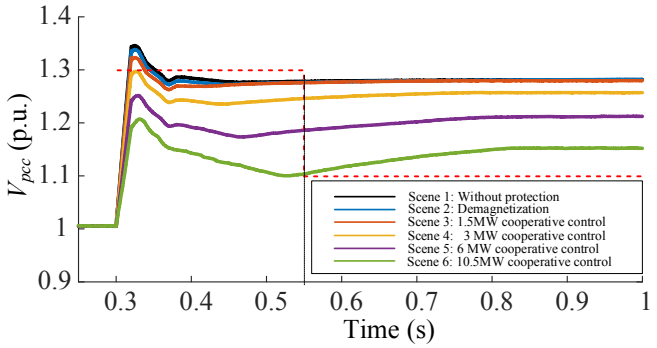

Fig. 9 Transient voltage at PCC under different scenes.

TABLE III
TRANSIENT VOLTAGE AT PCC UNDER DIFFERENT SCENES

Scene	Overvoltage (pu)	Scene	Overvoltage (pu)
1	1.345	4	1.2970
2	1.3386	5	1.2515
3	1.3232	6	1.1993

V. DISCUSSIONS ON FEASIBILITY & ECONOMICS OF SMES

Among various energy storage system, SMES have outstanding advantages of high efficiency, high power density, fast response, and long life cycle [33]-[34]. SMES stores energy in the form of electromagnetic energy in a superconducting magnet wound by superconducting tape and releases it through a power conditioning system (PCS) when needed. The zero resistance characteristic of superconducting tapes determines that SMES has the advantages of high efficiency; the high current density of superconducting tapes determines the high power density of SMES; It store power in the form of electromagnetic energy determines that SMES has the advantage of fast response, which typically in millisecond class; SMES has no electrochemical reactions and mechanical wear during operation, so it has long life circle. Therefore, SMES is very suitable for the applications of high power exchange and transient power compensation, such as fault ride through [35].

No matter in terms of power or capacity, there is no technical bottleneck for the development of SMES. Existing technology has been able to support the research and development of 100MW/1GJ level SMES. The obstacle that restricts the widespread use of SMES is cost, it is still relatively high nowadays. The price of second-generation high temperature superconducting (HTS) tape (YBCO) is about 10 times of copper wire [33].

TABLE IV
THE PRICE OF HTS TAPES IN THE PAST YEARS

	2010	2011	2014	2015	2016	2017
SUMITOMO	0.624	0.630	/	/	0.312	0.228
SuperPower	/	0.583	0.531	0.478	/	/
Shanghai Superconductor	/	/	/	0.213	0.191	0.182
AMSC	/	0.533	0.452	0.373	/	/

(YBCO $\A·m)

The SMES equipment costs contain four major parts: cold components costs (mainly are HTS magnet tapes costs), refrigeration costs, PCS costs, and operating costs.

The price of HTS tapes in the past years is shown in Table IV. Scholars from China predicted the potential costs change of SMES in [36]. With the development of manufacturing technology, the average tape price is expected to decline by 5-10% annually. According to the improvement in refrigerator efficiency and life cycle, the refrigeration costs are assumed to drop about 4.5% every year. Since PCS manufacturing is relatively mature, the PCS costs are assumed to reduce by 10% annually. Operating costs aare generally 5% of investment costs. In general, the SMES costs is showing a downward trend.

According to the statistics in [37], the total installed cost of 1.5 MW DFIG is about $ 1473 K in 2019. While the cost of the 0.3H/1750A SMES adopted in this paper is about $ 271.4 K. According to these estimations, the cost of SMES unit is about 12.28% of the 1.5 MW DFIG. As the SMES used still has a large margin, with the increase in the capacity of a single wind turbine [37], the ratio of SMES cost will be further greatly reduced. Besides, the ratio will continue to decline with the potential SMES cost reduction.

Several real projects on large-scale SMES have been put into operation. China has developed a 10 kV/1MVA/1MJ superconducting fault current limiter-magnetic energy storage system to improve the power output stability and the low voltage ride through capability of DFIG wind farms, which has been implemented in Gansu Province, China, showed excellent performance [38]. The successful implementation of this

project further proved the feasibility and effectiveness of SMES in renewable energy application.

The cost of SMES is still relatively high at present and SMES cannot be commercialized right now. However, considering the extremely attractive advantages of SMES and the future cost reduction, the application of SMES in the field of renewable energy has good prospects.

VI. Conclusion

In this paper, a cooperative strategy of SMES device and demagnetization control is proposed to enhance HVRT capability of DFIG-based wind farm under blocking fault of LCC-HVDC system. The main findings and contributions could be summarized as follows:

1) The proposed scheme coordinates the SMES with rotor side converter of DFIG to provide demagnetizing current to suppress key parameters of DFIG, as well as reactive current to mitigate the PCC overvoltage. Thus, the overall HVRT requirement of grid code can be completely satisfied.

2) The proposed scheme has been tested and demonstrated through several cases. The results have revealed that the proposed scheme can always maintain an acceptable level of electromagnetic torque and DC bus voltage. In converse, DC bus overvoltage and severe electromagnetic torque oscillation will occur in DFIG if any protection is not adopted.

3) Compared to the traditional demagnetization control, the main benefit of the proposed scheme is to provide more demagnetizing current and reactive current, due to the additional assistance of SMES. Consequently, better suppressing capability of DFIG parameters and PCC overvoltage can be obtained thus providing a favorable HVRT enhancement.

4) SMES costs is still relatively high nowadays but acceptable. Considering its extremely attractive advantages and the future cost reduction, the application of SMES in the field of renewable energy shows good prospects.

References

[1] Global Wind Energy Council (2020, Mar). *Global wind report 2019* [Online].
Available: http://gwec.net/global-wind-report-2019.

[2] J. Sun, M. Li, Z. Zhang, T. Xu, J.B. He, H. Wang, and G.H. Li, "Renewable energy transmission by HVDC across the continent: system challenges and opportunities," *CSEE Journal of Power and Energy Systems*, vol. 3, no. 4, pp. 353-364, Dec. 2017.

[3] Z. H. Liu, J. Yu, X. S. Guo, and T. Z. Sun. "Survey of technologies of line commutated converter based high voltage direct current transmission in China," *CSEE Journal of Power and Energy Systems*, vol. 1, no. 2, pp. 1-8, Jun. 2015.

[4] A. Yogarathinam, J. Kaur, and N. R. Chaudhuri, "Impact of inertia and effective short circuit ratio on control of frequency in weak grids interfacing LCC-HVDC and DFIG-based wind farms," *IEEE Transactions on Power Delivery*, vol. 32, no. 4, pp. 2040-2051, Aug. 2017.

[5] J. B. He, L. Wan, C. Huo, and Q. Chang, "Abnormal over-voltage risk analysis of HVDC transmission on atypical conditions," *Power System Technology*, vol. 38, no. 12, pp. 3459–63, Dec. 2014.

[6] C. Hong, "Mono-polar blocking fault analysis of Yunnan-Guangdong UHVDC system islanding operation," *Proceedings of the CSEE*, vol. 36, no. 7, pp. 1801-1807, Apr. 2016.

[7] I. Erlich, B. Paz, M. Koochack Zadeh, S. Vogt, C. Buchhagen, C. Rauscher, A. Menze, and J. Jung, "Overvoltage phenomena in offshore wind farms following blocking of the HVDC converter," in *2016 IEEE Power and Energy Society General Meeting (PESGM)*, Boston, MA, 2016, pp. 1-5.

[8] X. Z Luo, J. Zhang, J. B. He, C. Huo, J. M. Wang, Q. He, and A. S. Wang, "Coordinated control research of stability control system and pole control system under DC system block considering transient overvoltage" *Power System Technology*, vol. 39, no. 09, pp. 2526-2531, Sep. 2015.

[9] J. B. He, W. Zhuang, T. Xu, C. Huo, and W. Y. Jiang, "Study on cascading tripping risk of wind turbines caused by transient overvoltage and its countermeasures", *Power System Technology*, vol. 40, no. 06, pp. 1839-1844, Sep. 2015.

[10] H. Xu, W. Zhang, H. Nian, and J. Li, "Improved vector control of DFIG based wind turbine during grid dips and swells," in *2010 International Conference on Electrical Machines and Systems*, Incheon, 2010, pp. 511-515.

[11] Z. Xie, X. Zhang, X. Zhang, S. Yang, and L. Wang, "Improved ride-through control of DFIG during grid voltage swell," *IEEE Transactions on Industrial Electronics*, vol. 62, no. 6, pp. 3584-3594, Jun. 2015.

[12] M. Mohseni and S. M. Islam, "Transient control of DFIG-based wind power plants in compliance with the Australian grid code," *IEEE Transactions on Power Electronics*, vol. 27, no. 6, pp. 2813-2824, Jun. 2012.

[13] L. Y. Zhou, J. J. Liu, and S. Z. Zhou, "Demagnetization control for doubly-fed induction generator under balanced grid fault," *Power System Technology*, vol. 38, no. 12, pp. 3459–63, Dec. 2014.

[14] C. Zhou, Z. Wang, P. Ju and D. Gan, "High-voltage ride through strategy for DFIG considering converter blocking of HVDC system," *Journal of Modern Power Systems and Clean Energy*, vol. 8, no. 3, pp. 491-498, May. 2020.

[15] J. Yang, J. E. Fletcher, and J. O'Reilly, "A series dynamic resistor based converter protection scheme for doubly-fed induction generator during various fault conditions," *IEEE Transactions on Energy Conversion*, vol. 25, no. 2, pp. 422-432, Jun. 2010.

[16] S. G. Liasi, Z. Afshar, M. J. Harandi, and S. S. Kojori, "An improved control strategy for DVR in order to achieve both LVRT and HVRT in DFIG wind turbine," in *2018 International Conference and Exposition on Electrical and Power Engineering (EPE)*, Iasi, 2018, pp. 0724-0730.

[17] P. Dey, M. Datta, N. Fernando, and T. Senjyu, "Fault-ride-through performance improvement of a PMSG based wind energy systems via coordinated control of STATCOM," in *2018 IEEE International Conference on Industrial Technology (ICIT)*, Lyon, 2018, pp. 1236-1241.

[18] P. K. Dash, R. K. Patnaik, and S. P. Mishra, "Adaptive fractional integral terminal sliding mode power control of UPFC in DFIG wind farm penetrated multimachine power system," *Protection and Control of Modern Power Systems*, vol. 3, no. 1, pp. 1-14, Mar. 2018.

[19] H. Rezaie and M. H. Kazemi-Rahbar, "Enhancing voltage stability and LVRT capability of a wind-integrated power system using a fuzzy-based SVC," *Engineering Science and Technology-An International Journal-Jestech*, vol. 22, no. 3, pp.827-839, Jun. 2019.

[20] T. Zhang, J. Yao, J. X. Pei, Y. Luo, H. L. Zhang, K. Liu, and J. Wang," Coordinated control of HVDC sending system with large-scale DFIG-based wind farm under mono-polar blocking fault," *International Journal of Electrical Power & Energy Systems*, vol.119, Jul. 2020.

[21] P. P. Han, H. T. Zhang, M. Ding, Y. Zhang, L. Q. Chen, and B. B. Li,"A coordinated HVRT strategy of large-scale wind power transmitted with HVDC system," *Power System Technology*, vol. 42, no. 4, pp. 1086-1095, Apr. 2018.

[22] S. Y. Qin, R. R. Jiang, J. Liu, S. L. Li, L. W. Dai, and Q. Liu," Transient overvoltage analysis of wind farm with UHVDC block and HVRT coordinated control," *Electric Power Automation Equipment*, vol. 40, no. 06, pp. 63-69+1-4, Jun. 2020.

[23] N. Amaro, J. M. Pina, J. Martins, and J. M. Ceballos, "Integration of SMES devices in power systems - opportunities and challenges," in *2015 9th International Conference on Compatibility and Power Electronics (CPE)*, Costa da Caparica, 2015, pp. 482-487.

[24] B. Zakeri and S. Syri," Electrical energy storage systems: A comparative life cycle cost analysis," *Renewable & Sustainable Energy Reviews*, vol. 42, pp. 569-596, Feb. 2015.

[25] Q. Huang, X. Zou, D. Zhu, and Y. Kang, "Scaled current tracking control for doubly fed induction generator to ride-through serious grid faults," *IEEE Transactions on Power Electronics*, vol. 31, no. 3, pp. 2150-2165, Mar. 2016.

[26] A. M. S. Yunus, M. A. S. Masoum, and A. Abu-Siada, "Application of SMES to enhance the dynamic performance of DFIG during voltage sag

and swell," *IEEE Transactions on Applied Superconductivity*, vol. 22, no. 4, pp. 5702009-5702009, Aug. 2012,
[27] J. H. Liu, H. Zhang, J. Li, B. H. Yang, and Y. Min," Application of SMES to improve fault voltage ride through capability of doubly fed induction generator," *Transactions of China Electrotechnical Society*, vol. 30, no. 22, pp. 199-205, Nov. 2015.
[28] F. Wang, T. Q. Liu, Y. Y. Ding, Q. Zeng, and X. Y. Li, "Calculation method and influencing factors of transient overvoltage caused by HVDC block," *Power System Technology*, vol. 40, no. 10, pp. 3059-3065, Oct. 2016.
[29] Y. Q. Liang, "A new time domain positive and negative sequence component decomposition algorithm," in *2003 IEEE Power Engineering Society General Meeting*, Toronto, Ont., 2003, pp. 1638-1643.
[30] X. Xiao, R. Yang, Z. Zheng, and Y. Wang, "Cooperative rotor-side SMES and transient control for improving the LVRT capability of grid-connected DFIG-based wind farm," *IEEE Transactions on Applied Superconductivity*, vol. 29, no. 2, pp. 1-5, Mar. 2019.
[31] Z. Zheng, X. Xiao, X. Y. Chen, C. Huang, and J. Xu, "Performance evaluation of a MW-class SMES-based DVR system for enhancing transient voltage quality by using d–q transform control," *IEEE Transactions on Applied Superconductivity*, vol. 28, no. 4, pp. 1-5, Jun. 2018.
[32] Z. Zheng, X. Xiao, X. Chen, C. Huang, L. Zhao and C. Li, "Performance evaluation of a MW-class SMES-BES DVR system for mitigation of voltage quality disturbances," *IEEE Transactions on Industry Applications*, vol. 54, no. 4, pp. 3090-3099, July-Aug. 2018.
[33] W. Y. Guo, F. Y. Cai, C. Zhao, J. Y. Zhang, Y. P. Teng, and L. Y. Xiao," Application and prospect of superconducting magnetic energy storage for renewable energy," *Automation of Electric Power Systems*, vol. 43, no. 8, pp. 2-19, Apr. 2019.
[34] X. Luo, J. H. Wang, M. Dooner, and J. Clarke," Overview of current development in electrical energy storage technologies and the application potential in power system operation," *Applied Energy*, vol. 137, pp. 511-536, Jan. 2015.
[35] T. Karaipoom and I. Ngamroo, "Optimal superconducting coil integrated into DFIG wind turbine for fault ride through capability enhancement and output power fluctuation suppression," *IEEE Transactions on Sustainable Energy*, vol. 6, no. 1, pp. 28-42, Jan. 2015.
[36] X. Zhou, Y. J. Tang, J. Shi, C. Zhang, K. Gong, L. H. Zhang, and Y. Y. Li, "Cost estimation models of MJ class HTS superconducting magnetic energy storage magnets," *IEEE Transactions on Applied Superconductivity*, vol. 28, no. 4, pp. 1-5, Jun. 2018.
[37] International Renewable Energy Agency (2020, Jun). Renewable power generation costs in 2019. [Online]. Available:https://www.irena.org/publications/2020/Jun/Renewable-Power-Costs-in-2019.
[38] W. Y. Guo, G. M. Zhang, J. Y. Zhang, N. H. Song, Z. Y. Gao, X. Xu, L. W. Jing, and Y. P. Teng, "Development of a 1-MVA/1-MJ superconducting fault current limiter–magnetic energy storage system for LVRT capability enhancement and wind power smoothing," *IEEE Transactions on Applied Superconductivity*, vol. 28, no. 4, pp. 1-5, Jun. 2018.

Qi Xie received the B.Eng. degree in electrical engineering and its automation from Sichuan University, Chengdu, China, in 2019, where he is currently working toward the M.SC. degree in electrical engineering. His research interests include power quality and renewable energy.

Zixuan Zheng (M'17) received the B.S. and Ph.D. degrees in electrical engineering from Sichuan University, Chengdu, China, in 2012 and 2017, respectively. He is currently a Postdoctoral Fellow with the College of Electrical Engineering, Sichuan University. His research interests include power quality, operation and control of distributed energy resources.

Xianyong Xiao (M'07–SM'16) received the B.S., M.S., and Ph.D. degrees in electrical engineering from Sichuan University, Chengdu, China, in 1990, 1998, and 2010, respectively. He is currently a Professor with the College of Electrical Engineering, Sichuan University. His research interests include power quality, smart distribution system, power system catastrophic event, uncertainty theory, and uncertain measure applied to power systems.

Chunjun Huang received the B.S., M.S. degrees in electrical engineering from Sichuan University, Chengdu, China, in 2017 and 2020, respectively. He is currently working toward the Ph.D. degree with the Center for Electric Power and Energy, Technical University of Denmark. His research interests include renewable energy generation, energy storage system and integrated energy system.

Jiaqu Zheng received the B.Eng. degree in electrical engineering and its automation, in 2017. He is currently working toward the M.SC. degree in electrical engineering in Sichuan University. His research interest is renewable energy.

Jie Ren received the B.S. degree in electrical engineering and its automation from Sichuan University, Chengdu, China, in 2017, where she is currently working toward the Ph.D. degree in power system and its automation. Her research interests include renewable energy generation and fault ride through of wind turbine generator.